On the magnetism of $Ln_{2/3}Cu_3Ti_4O_{12}$ (Ln = lanthanide)

A. Dittl[1], S. Krohns[1,a], J. Sebald[1], F. Schrettle[1], M. Hemmida[1], H.-A. Krug von Nidda[1], S. Riegg[1], A. Reller[2], S. G. Ebbinghaus[3], and A. Loidl[1]

[1] Experimental Physics V, Center for Electronic Correlations and Magnetism, University of Augsburg, 86135 Augsburg, Germany
[2] Resource Strategy, University of Augsburg, 86135 Augsburg, Germany
[3] Solid State Chemistry, Martin-Luther University Halle-Wittenberg, 06120 Halle, Germany

August 27, 2018

Abstract. The magnetic and thermodynamic properties of the complete $Ln_{2/3}Cu_3Ti_4O_{12}$ series were investigated. Here Ln stands for the lanthanides La, Ce, Pr, Nd, Sm, Eu, Gd, Tb, Dy, Ho, Er, Tm, and Yb. All the samples investigated crystallize in the space group $Im\bar{3}$ with lattice constants that follow the lanthanide contraction. The lattice constant of the Ce compound reveals the presence of Ce^{4+} leading to the composition $Ce_{1/2}Cu_3Ti_4O_{12}$. From magnetic susceptibility and electron-spin resonance experiments it can be concluded that the copper ions always carry a spin $S = 1/2$ and order antiferromagnetically close to 25 K. The Curie-Weiss temperatures can approximately be calculated assuming a two-sublattice model corresponding to the copper and lanthanide ions, respectively. It seems that the magnetic moments of the heavy rare earths are weakly coupled to the copper spins, while for the light lanthanides no such coupling was found. The $4f$ moments remain paramagnetic down to the lowest temperatures, with the exception of the Tm compound, which indicates enhanced Van-Vleck magnetism due to a non-magnetic singlet ground state of the crystal-field split $4f$ manifold. From specific-heat measurements we accurately determined the antiferromagnetic ordering temperature and obtained information on the crystal-field states of the rare-earth ions. The heat-capacity results also revealed the presence of a small fraction of Ce^{3+} in a magnetic $4f^1$ state.

PACS. XX.XX.XX No PACS code given

1 Introduction

Perovskite derived oxides of $AC_3B_4O_{12}$ type constitute a broad new class of compounds with fascinating properties. When three fourths of the A-site ions of the parent perovskite ABO_3 are substituted by a Jahn-Teller active ion, like Cu^{2+} or Mn^{3+}, a collective rotation of the BO_6 octahedra around the crystallographic (111) axis gives rise to a square-planar coordination of these ions. Thus, the cubic lattice parameter doubles along all three directions resulting in an eight times larger unit cell. These compounds are described by the stoichiometry $AC_3B_4O_{12}$. Here the C-site cations possess a square-planar oxygen coordination analogous to the Cu–O planes in the high-T_c superconducting cuprates. In the $AC_3B_4O_{12}$ structure a large variety of cations, irrespective of the nominal charge state, can be substituted in the icosahedral environment of the A site, namely monovalent Na^+, divalent Ca^{2+}, Sr^{2+}, Cd^{2+}, as well as trivalent Y^{3+} and any lanthanide element from La^{3+} to Lu^{3+} and – as will be shown later – even tetravalent Ce^{4+}. As mentioned above, the C positions are occupied by Jahn-Teller active ions which strongly distort the perovskite structure by concomitant orbital order. Finally, the B site can be occupied by a large variety of transition- and main-group metal ions, like e.g. Mn^{3+}, Fe^{3+}, Ti^{4+}, and Ru^{4+}, to name the most prominent examples. For a review on this class of new materials see Ref. [1]. Recently $CaCu_3Ti_4O_{12}$ gained considerable attention with respect to reported colossal values of the dielectric constants [2, 3,4,5,6]. $CaCu_3Mn_4O_{12}$ is a semiconducting ferromagnet with an ordering temperature as high as 360 K revealing large magneto-resistance effects [7,8]. Heavy-fermion behavior [9,10,11] has been reported for $CaCu_3Ru_4O_{12}$ as well as for $LnCu_3Ru_4O_{12}$ (Ln = La, Pr, Nd) [12] and finally a temperature induced valence transition accompanied by a metal-to-insulator transition has been found in $LaCu_3Fe_4O_{12}$ [13].

Here we focus on the magnetic properties of the insulating $Ln_{2/3}Cu_3Ti_4O_{12}$ compounds, where Ln stands for any rare-earth element except Lu and the radioactive Pm. The synthesis of these oxides has first been reported by Deschanvres *et al.* [14] and Bochu *et al.* [15]. For charge neutrality one third of the A sites remains vacant. Dielectric properties of this class of materials were published by Subramanian *et al.* [3,16], Liu *et al.* [17]

[a] e-mail: stephan.krohns@physik.uni-augsburg.de

and Sebald *et al.* [18], discussing the colossal values of the dielectric constant similar to $CaCu_3Ti_4O_{12}$. However, to the best of our knowledge no reports are available on magnetisation and specific heat of $Ln_{2/3}Cu_3Ti_4O_{12}$ where rare-earth magnetic moments are introduced in addition to the Cu spins. Usually the Cu^{2+} subsystem in insulating $ACu_3Ti_4O_{12}$ behaves simple: As documented for $CaCu_3Ti_4O_{12}$, the copper ions are in a $3d^9$ electronic configuration with spin $S = 1/2$. They mainly interact via the neighboring titanium and oxygen ions by super-exchange interactions, thereby constituting a Curie-Weiss temperature which ranges between -34 K and -41 K, depending on synthesis conditions [19,20]. $CaCu_3Ti_4O_{12}$ undergoes antiferromagnetic (AFM) order with a collinear spin arrangement at $T_N = 25$ K [21]. The onset of magnetic ordering is associated with a well-defined lambda-type anomaly in the specific heat [22]. As Curie-Weiss temperature and ordering temperature are of the same order of magnitude, the copper spins obviously are not frustrated.

In the rare-earth compounds the coupling between copper and rare-earth ions is expected to be weak due to the small overlap of the $4f$ shell with the neighboring ions. Therefore to first approximation, the ordering temperature should be independent of the rare-earth spins. For the same reason the coupling between the rare-earth ions will be even weaker and the corresponding super-exchange is negligible. However, when substituting Ti ions by Ru, the system undergoes a metal-to-insulator transition, where the localized Cu moments vanish and the compounds become metallic with heavy-quasiparticle properties [23]. For the Ti rich side thermoelectric power was found to be strongly dependent on the *Ln* ions indicating an increasing hybridization between Cu $3d$ and Ru $4d$ electrons with decreasing radius of the *Ln* ion [24]. From this point of view it is important to systematically investigate the magnetic properties of the pure $Ln_{2/3}Cu_3Ti_4O_{12}$ compounds which will be one starting point for further experiments with solid solutions between titanium and ruthenium compounds.

In this work the structural data of polycrystalline $Ln_{2/3}Cu_3Ti_4O_{12}$ compounds, with *Ln* = La, Ce, Pr, Nd, Sm, Eu, Gd, Tb, Dy, Ho, Er, Tm, and Yb are presented. We studied the magnetic bulk properties by SQUID measurements, while electron-spin resonance (ESR) experiments were utilized to probe the local environment of copper spins and rare-earth moments. The specific-heat measurements provided a precise measure of the magnetic ordering temperature and of the crystal-field states of the rare-earth ions.

2 Sample preparation and experimental details

Polycrystalline samples of $Ln_{2/3}Cu_3Ti_4O_{12}$ were prepared by solid-state reaction. CuO, TiO_2, and the binary oxides, Ln_2O_3 – with the exception of Pr_6O_{11}, CeO_2, and Tb_4O_7 – were mixed in corresponding molar ratios and were well ground in an agate mortar. Before weighting, all lanthanide oxides were dried at 900°C for 12 h to remove any water from the samples. In the same way, Pr_2O_3 was reacted to non-hygroscopic Pr_6O_{11}. An excess of 0.3 g - 0.4 g CuO was added as flux material. After completion of the reaction, this excess was removed by washing the samples with hydrochloride acid (10%) and afterwards with deionized water. Before calcination, the samples were pressed into pellets. Calcination in aluminum-oxide crucibles was performed in two steps, first at 1000°C for 48 h in air with subsequent regrinding followed by a second heating to 1025°C again for 48 h in air.

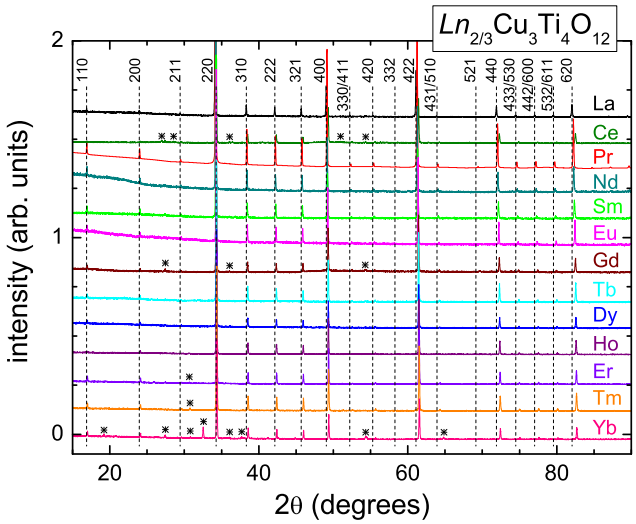

Fig. 1. (Color online) Diffraction pattern of all lanthanide compounds investigated in this work, vertically shifted for clarity. Vertical dashed lines indicate the Bragg reflections of $La_{2/3}Cu_3Ti_4O_{12}$ and document the lanthanide contraction. Asterisks denote impurity phases. The Miller indices of all Bragg reflections are given on top of the figure.

The x-ray diffraction experiments were performed on a Seifert 3003 TT powder diffractometer using Cu-K_α radiation. To provide qualitative information on the sample quality, Figure 1 shows the diffraction profiles of all lanthanide compounds investigated from lanthanum (top) to ytterbium (bottom). The Bragg reflections are indexed on top of the figure. Most of the $Ln_{2/3}Cu_3Ti_4O_{12}$ compounds are single-phase within the detection limit of XRD. Peaks, which are due to impurity phases, are indicated by asterisks. Only $Yb_{2/3}Cu_3Ti_4O_{12}$ and $Ce_{1/2}Cu_3Ti_4O_{12}$ exhibit a considerable amount of impurity phases and specifically in the Yb sample a well developed Bragg reflection due to a foreign phase shows up close to 33°. Traces of impurity peaks with marginal intensity appear in the Gd, Er, and Tm compounds. The dashed lines indicate the scattering angles of the Bragg reflections of $La_{2/3}Cu_3Ti_4O_{12}$. At large scattering angles the lanthanide contraction of the series can easily be detected from the increasing shift of the Bragg reflections to higher angles with increasing atomic number. Moreover, one observes that in $Ce_{1/2}Cu_3Ti_4O_{12}$ the Bragg peaks appear at too large scattering angles indicating a smaller cell volume than expected. This is a hint, that Ce possibly is in a tetravalent

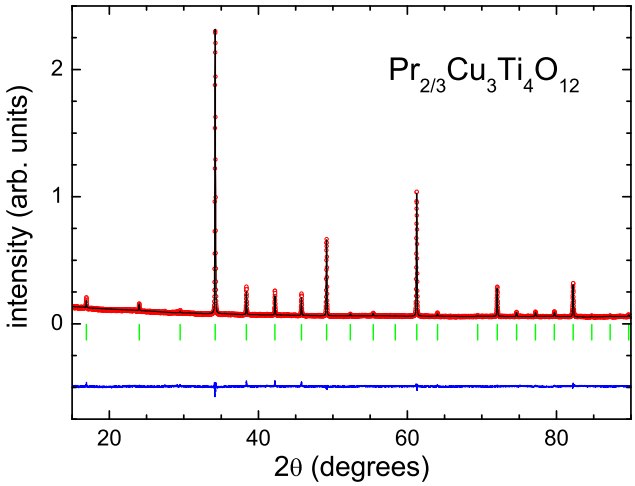

Fig. 2. (Color online) Diffraction profile (empty symbols) and Rietveld refinement (solid line) for $Pr_{2/3}Cu_3Ti_4O_{12}$. The vertical bars indicate the angular positions of the expected Bragg reflections. The difference pattern between calculated and measured profile at the bottom is shifted by -0.5 for clarity.

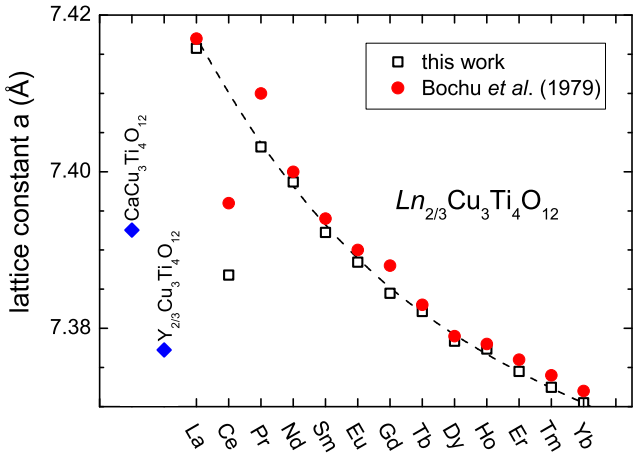

Fig. 3. (Color online) Evolution of the lattice constants of the lanthanide series (empty squares). The lattice constants of the isostructural Ca and Y compound are also indicated. Expermimental results from Bochu *et al.* [15] are plotted for comparison (full red circles). The dashed line is drawn to guide the eye and provides a smooth extrapolation of the trivalent compounds.

state, as already concluded in the early work by Bochu *et al.* [15].

To provide quantitative information on lattice constants and on sample quality, all diffraction patterns were refined within space group $Im\bar{3}$ using the Rietveld method, resulting in R values well below 5%. As a representative example, Fig. 2 shows the diffraction profile including the Rietveld refinement for $Pr_{2/3}Cu_3Ti_4O_{12}$. The angular positions of the expected Bragg reflections are indicated by vertical bars. The difference pattern proves the excellent fit and, thus, the phase purity of the sample.

The evolution of the lattice parameter is documented in Fig. 3 for the complete lanthanide series in comparison with published results by Bochu *et al.* [15]. Except for $Ce_{1/2}Cu_3Ti_4O_{12}$ and $Pr_{2/3}Cu_3Ti_4O_{12}$ the agreement is excellent. In addition the lattice constants of $CaCu_3Ti_4O_{12}$ and $Y_{2/3}Cu_3Ti_4O_{12}$, which have been prepared in the course of this work, are also shown. The cell parameters continuously decrease on increasing atomic number from 7.416 Å for La to 7.371 Å for Yb due to the lanthanide contraction. However, a decrease by 0.045 Å is rather small, as the ionic radii of the trivalent compounds (e.g., in octahedral symmetry) decrease from 1.03 Å for La^{3+} to 0.87 Å for Yb^{3+}. This fact indicates that the available space for the A cations is rather fixed and determined from the strong tilting of the TiO_6 octahedra.

The lattice constant for the Ce compound is too small compared to the continuous evolution along the lanthanide series. Often cerium is found to exhibit a $4f^0$ configuration and in this case the ionic radius decreases from 1.01 Å for the trivalent ion to 0.87 Å for Ce^{4+}. According to x-ray diffraction the majority of the cerium ions seems to have the valence 4+ and the stoichiometry of this compound probably has to be written as $Ce_{1/2}Cu_3Ti_4O_{12}$, if one assumes strict charge neutrality. This means that in this structure half of the A sites are occupied by vacancies. So far we were not able to synthesize $Ce_{1/2}Cu_3Ti_4O_{12}$ in pure form without impurity phases. On the other hand for the Ce compounds investigated the impurity phase does not exceed 5%.

In the further course of this work we investigated the magnetic properties and the specific heat. The dc magnetic susceptibility has been studied in a temperature range $1.8 \leq T \leq 400$ K utilizing a commercial Superconducting Quantum Interference Device magnetometer (MPMS-5, Quantum Design). The heat capacity was measured in a Physical Properties Measurements System (PPMS, Quantum Design) for temperatures between 1.8 K and 50 K. In the specific-heat measurements we focused on the low temperatures to get information on the magnetic ordering, crystal-field excitations of the rare-earth ions, and of the low-temperature phonon properties. The ESR experiments were performed in a Bruker ELEXSYS E500 CW spectrometer at X-band frequency (9.4 GHz). This ESR spectrometer is equipped with a continuous He-gas flow cryostat (Oxford instruments) working in the temperature range from liquid helium to room temperature.

3 Experimental Results and Discussion

3.1 Magnetic susceptibility

Figure 4 depicts the magnetic susceptibility as function of temperature for all lanthanide compounds from La to Yb in an external magnetic field of 1000 Oe and between 1.8 K and 400 K. The upper frame shows the susceptibility, the lower frame the inverse susceptibility. The symbols characterizing the different compounds are indicated in the upper frame. Starting the discussion with the lower frame first, one observes that all compounds exhibit a well defined Curie-Weiss like susceptibility for $T > 50$ K. Three groups of lines with different slopes can be distinguished:

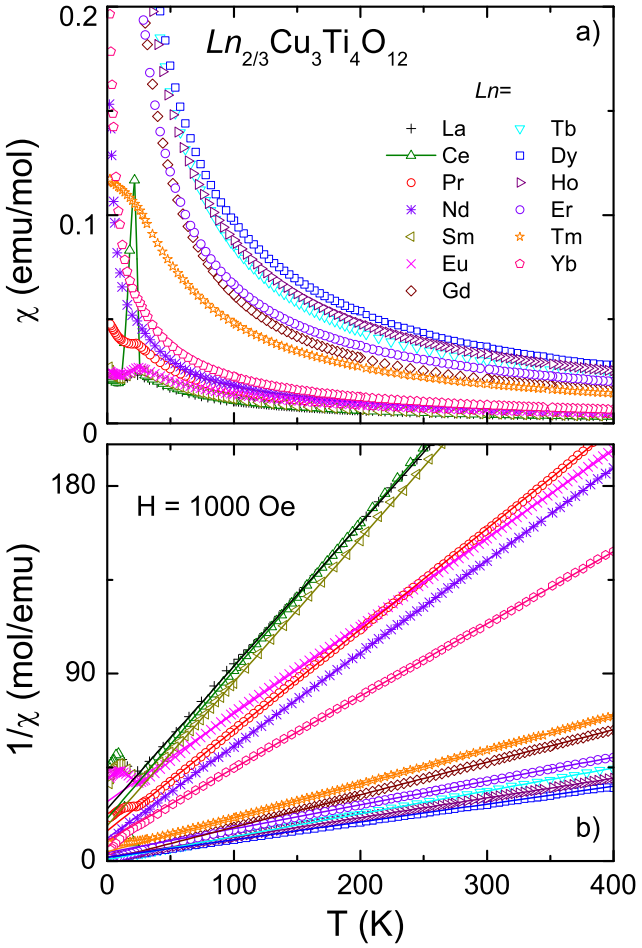

Fig. 4. (Color online) Magnetic susceptibility measured at $H = 1000\,\mathrm{Oe}$ of all $Ln_{2/3}Cu_3Ti_4O_{12}$ compounds. a) Susceptibility vs. temperature. b) Inverse susceptibility vs. temperature. The solid lines in the lower frame correspond to Curie-Weiss fits as described in the text. Symbols characterizing the different Ln compounds are indicated in the upper frame.

The samples with Ln = La, Ce, Sm exhibit the steepest slopes. In these cases the transitions into long-range AFM order are clearly visible close to 25 K. Naturally, for Ln = La the slope is solely determined by the spin $S = 1/2$ of the copper ions. The approximate coincidence of the susceptibilities of the La and the Ce compounds demonstrates that the majority of cerium ions is in the non magnetic $4f^0$ state. For Sm^{3+} the effective magnetic moment is small compared to that of Cu^{2+}, therefore, the three copper ions per formula unit dominate the susceptibility of this oxide. The lowest slopes are found for the heavy rare earths (Ln = Tm, Gd, Er, Tb, Ho and Dy). For these compounds the large moment of the rare-earth ion governs the susceptibility down to the lowest temperature and even the AFM transition of the copper ions is hidden by the large paramagnetic susceptibility. Finally in between these two extremes, we find the compounds (Ln = Pr, Nd, Eu, and Yb) where the rare-earth moment (only 2/3 per formula unit) and the copper spins (3 Cu ions per unit cell) are of comparable magnitude.

Turning now to the upper frame we find two further significant differences in the temperature dependent magnetic susceptibilities of $Ln_{2/3}Cu_3Ti_4O_{12}$. The Tm compound reveals a saturation towards low temperatures indicating the existence of a non-magnetic ground state. This situation sometimes occurs for Tm and Pr compounds in a cubic crystal field. In these cases the crystal-field splitting of the rare-earth moment leads to a non-magnetic singlet ground state. Thus, the susceptibility at low temperatures is of Van-Vleck type due to the polarization of the singlet ground state [25]. Secondly, $Ce_{1/2}Cu_3Ti_4O_{12}$ exhibits a much more significant and enhanced anomaly at the AFM ordering transition of the copper spins.

For a more quantitative analysis we fitted the susceptibility data of all compounds for $50 < T < 400\,\mathrm{K}$ by a Curie-Weiss law

$$\chi = \frac{N_\mathrm{A}\mu_\mathrm{eff}^2}{3k_\mathrm{B}(T-\Theta_\mathrm{CW})} + \chi_0 \qquad (1)$$

(with Avogadro number N_A and Boltzmann constant k_B). In these fits we included also a temperature independent term χ_0 representing possible diamagnetic behavior or Van Vleck type paramagnetism. The fits yielded positive Van Vleck like contributions of the order of 10^{-4} - 10^{-3} emu/mol for all samples. Compared to the overall size of the susceptibility as shown in the upper frame of Fig. 4, these contributions seem to be rather negligible. The resulting Curie-Weiss temperatures, Θ_CW, and paramagnetic effective moments, μ_eff, are depicted in Figure 5. The theoretically expected effective paramagnetic moments for $Ln_{2/3}Cu_3Ti_4O_{12}$ are calculated via

$$\mu_\mathrm{eff}^2 = \frac{2}{3}\mu_\mathrm{eff}^2(Ln) + 3\mu_\mathrm{eff}^2(\mathrm{Cu}). \qquad (2)$$

In the lower frame of Fig. 5, the measured values (full blue diamonds) were analyzed using the following procedure: we calculated the rare-earth moments according to Hund's rule coupling assuming that at high temperatures all crystal-field levels are occupied and the rare-earth ions exhibit their full moment. These calculated values are indicated as full (green) squares. In these calculations we assumed a non-magnetic $4f^0$ state for the cerium compound. These values were subtracted from the measured effective moments to give the average spin moment per copper ion over the complete series of lanthanide compounds (full red circles). As can be seen, these values slightly scatter around roughly 2.0 μ_B yielding an average effective moment of 1.920 μ_B per copper ion. This results in a g value of 2.22 which is enhanced by spin-orbit coupling with respect to the spin–only value as typical for Cu–$3d^9$ systems. From this figure it is evident that the assumption of non-magnetic cerium describes the results satisfactorily.

The experimental Curie-Weiss temperatures depicted in the upper frame of Fig. 5 have to be compared to the theoretically expected values, which for a two-sublattice antiferromagnet can easily be calculated using

$$\Theta_\mathrm{CW} = \frac{2\lambda_{AB}C_AC_B - \lambda_{AA}C_A^2 - \lambda_{BB}C_B^2}{C_A + C_B}. \qquad (3)$$

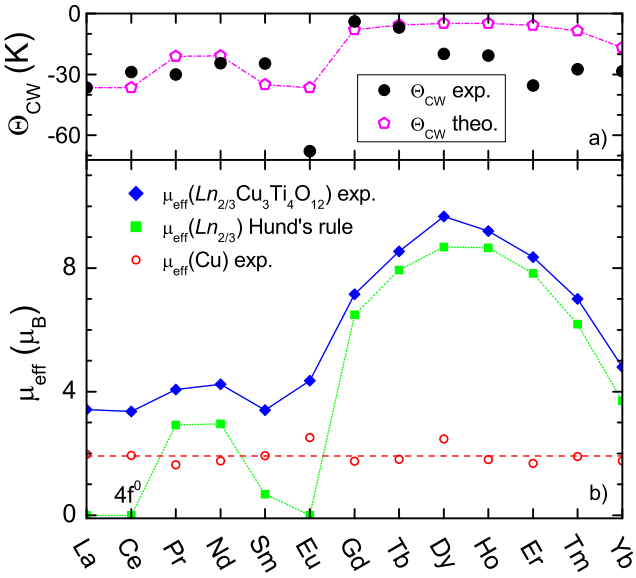

Fig. 5. a) Experimental Curie-Weiss temperatures (full black circles) of $Ln_{2/3}Cu_3Ti_4O_{12}$ as determined from high-temperature Curie-Weiss fits as shown in Fig. 4 compared to calculated Curie-Weiss temperatures (empty red circles) as described in the text. The dash-dotted line is drawn to guide the eye. b) Effective moments as determined from the paramagnetic high-temperature behavior (full blue diamonds). Calculated moments of the rare-earth ions according to Hund's rule coupling (full green squares) are presented in addition to the calculated effective Cu moments for the $Ln_{2/3}Cu_3Ti_4O_{12}$ compounds (empty red symbols). Solid and dotted lines are drawn to guide the eye. The dashed line is the average effective copper moment.

Here C_A and C_B are the Curie constants of the A (Cu) and of the B (rare-earth ions) sublattice, respectively. λ_{ij} are the effective coupling constants within the sublattices A and B and in between these two sublattices. As first approximation it is reasonable to assume that in $Ln_{2/3}Cu_3Ti_4O_{12}$ the rare-earth ions are fully decoupled yielding $\lambda_{BB} = 0$ and that also the coupling between the Cu and lanthanide ions is weak, resulting in $\lambda_{AB} \sim 0$. In this case the Curie-Weiss temperature is only given by $\Theta_{\rm CW} = -\lambda_{AA}C_A^2/(C_A + C_B)$. In the La compound with only one sublattice one obtains $\Theta_{\rm CW} = -\lambda_{AA}C_A = -37.0\,$K, very close to the values found in $CaCu_3Ti_4O_{12}$ [19]. Calculating the Curie-Weiss temperatures for the complete lanthanide series using the effective moments for the rare-earth ions as indicated in the lower frame of Fig. 5, gives the magenta open pentagons which are plotted in the upper frame of Fig. 5. The agreement is satisfactory with the exception of the Eu compound and the heavy rare earths. It seems that in the latter case the coupling between the rare-earth and the copper spin system cannot be fully neglected.

For $Eu_{2/3}Cu_3Ti_4O_{12}$ we additionally found an enhanced Curie-Weiss temperature $\Theta_{\rm CW} = -68\,$K and a significantly smaller slope than for $La_{2/3}Cu_3Ti_4O_{12}$, although the magnetic moment of Eu^{3+} vanishes in the ground state with zero total moment $J = 0$. This is a general observation for magnetic compounds containing Eu^{3+}, like e.g. $EuMnO_3$ [26], and results from the thermal occupation of the excited $J = 1$ state of the europium ion yielding a temperature-dependent van-Vleck contribution of the susceptibility at elevated temperatures, which effectively enhances paramagnetic moment and Curie-Weiss temperature.

3.2 Specific heat

For a number of $Ln_{2/3}Cu_3Ti_4O_{12}$ compounds we measured the heat capacity between 2 K and 50 K. Besides $La_{2/3}Cu_3Ti_4O_{12}$, we selected representative light and heavy rare-earth compounds which behave rather unusual in the temperature dependent magnetic susceptibility. In addition we wanted to check the magnetic ordering temperatures, as these can hardly be identified in the compounds with heavy rare earths (see Fig. 4). Figure 6 shows the measured heat capacities for $Ln_{2/3}Cu_3Ti_4O_{12}$ with Ln = La, Ce, Pr, Eu, Ho, and Tm plotted as C/T vs. T. At first sight it is evident that all compounds reveal antiferromagnetic order close to 25 K similar to $CaCu_3Ti_4O_{12}$ [21]. At this temperature the copper spins with $S = 1/2$ undergo long-range AFM order. It is interesting to note that the ordering temperatures shift from 22.5 K for the La to 25 K for the Tm compound and it seems that the heavy rare-earth compounds exhibit slightly higher ordering temperatures. Obviously the heavy rare-earth compounds exhibit non-vanishing exchange between the copper spins and the $4f$ moments, a fact that also seems to be supported by the evolution of the Curie-Weiss temperatures documented in the upper frame of Fig. 5. An alternative explanation could be found in the lanthanide contraction slightly enhancing the superexchange between neighboring copper ions.

In some of the systems crystal-field excitations can easily be recognized. $Ho_{2/3}Cu_3Ti_4O_{12}$ and astonishingly $Ce_{1/2}Cu_3Ti_4O_{12}$ exhibit a well defined hump at 5 K indicating low-lying crystal-field excitations. In case of the cerium compounds this has been rather unexpected as from the diffraction and susceptibility experiments the cerium ion has been characterized as $4f^0$, i.e. non magnetic. However, Fig. 6 proves that a certain fraction of cerium ions is definitely in the $4f^1$ state. The anomaly for Ln = Ho is significantly larger than for the Ce. Therefore we conclude that only a small fraction is in the Ce^{3+} state. The heat-capacity contributions due to the crystal-field excitations of $Pr_{2/3}Cu_3Ti_4O_{12}$ and of the singlet-ground state in $Tm_{2/3}Cu_3Ti_4O_{12}$ extend over larger temperature ranges, i.e. from 2 K to almost 40 K and from 10 K to temperatures well above 50 K, respectively. Of course, no $4f$-derived crystal-field excitations are visible in the compounds with non-magnetic A-site $La_{2/3}Cu_3Ti_4O_{12}$ and $Eu_{2/3}Cu_3Ti_4O_{12}$.

To get a more quantitative estimate of the $4f$ derived contributions to the heat capacity for all compounds with rare-earth crystal-field excitations, we subtracted the specific heat of $La_{2/3}Cu_3Ti_4O_{12}$. This accounts for the pure phonon density of states and for the heat capacity of the

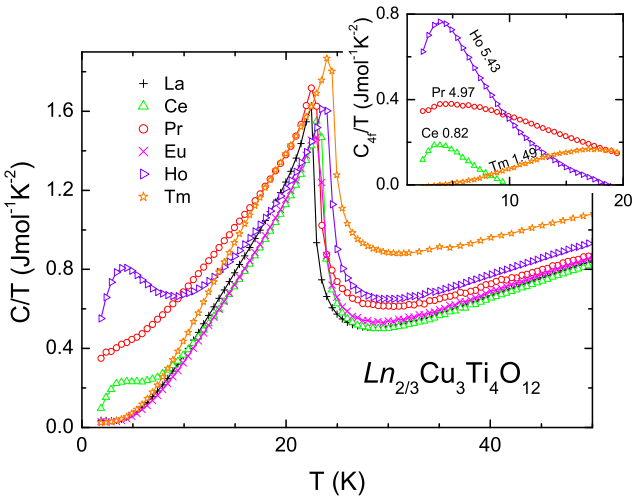

Fig. 6. Heat capacity of $Ln_{2/3}Cu_3Ti_4O_{12}$ with Ln = La, Ce, Pr, Eu, Ho, and Tm the heat capacity is plotted as C/T *vs* temperature. Symbols are indicated within the frame. The solid lines are drawn to guide the eye. Inset: Rare-earth derived magnetic heat capacities of $Ln_{2/3}Cu_3Ti_4O_{12}$ for Ln = Ce, Pr, Ho, and Tm, plotted as C/T *vs* T. To determine the contribution of rare-earth ions the heat capacity of $La_{2/3}Cu_3Ti_4O_{12}$ has been subtracted from the measured heat capacities shown in the main frame. The entropies due to the crystal-field excitations have been estimated for the temperature regime $2 < T < 20$ K and are indicated in the figure in units of J mol^{-1} K^{-1}.

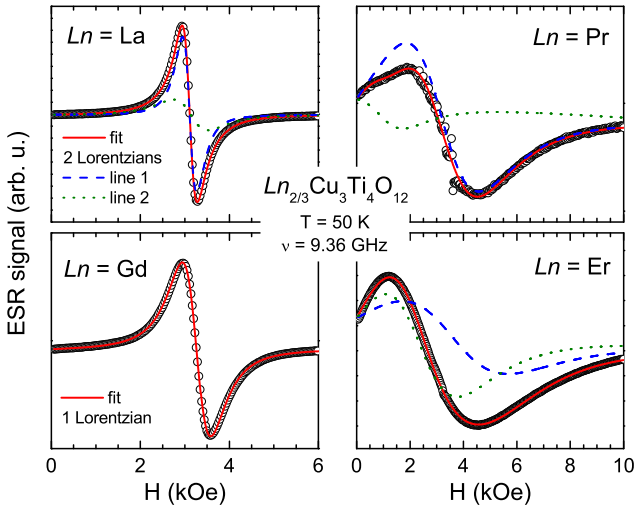

Fig. 7. (Color online) Selected ESR-Spectra of $Ln_{2/3}Cu_3Ti_4O_{12}$ taken at 50 K with Ln = La, Gd, Pr, and Er. Solid lines indicate the fits, dashed and dotted lines illustrate the different contributions for fits with two Lorentzians.

ordering copper spin system. The results are documented in the inset of Fig. 6 and represent an estimate of the heat capacity due to the $4f$ moments. Here we show C/T vs T between 2 K and 20 K for $Ln_{2/3}Cu_3Ti_4O_{12}$ with Ln = Ce, Pr, Ho, and Tm. The corresponding entropy values are indicated at the plotted anomalies in units of J mol^{-1} K^{-1}. Having in mind that in the regular structure only 2/3 of the A sites are occupied by rare-earth ions, the entropies correspond to triplet states for the Ho and Pr compounds and roughly to a singlet-singlet transition for the Tm compound. Assuming that the crystal-field anomaly for $Ce_{1/2}Cu_3Ti_4O_{12}$ corresponds to a transition within a doublet, we conclude that about 10% of the A sites would be occupied by trivalent cerium, 40% by tetravalent cerium and 50% would remain empty. Note that to obtain charge neutrality, in this case the Ce occupation of the A site has to be about 55%. Of course we cannot exclude that these crystal-field contributions result from another cerium-containing phase. However, a value of 10% impurity phase seems to be too large, specifically when inspecting the diffractogram as indicated in Fig. 1.

3.3 Electron spin resonance

A complementary and microscopic access to the magnetic properties is provided via electron spin resonance (ESR) which detects the microwave absorption due to magnetic dipolar transitions between the Zeeman levels of the magnetic ions. The ESR spectra are taken at constant microwave frequency $\nu \approx 9.4$ GHz dependent on the external static magnetic field H. Due to the lock-in technique with field modulation the field derivative of the absorption signal is recorded. Figure 7 shows representative examples of ESR spectra obtained in $Ln_{2/3}Cu_3Ti_4O_{12}$ with different rare-earth ions: Four characteristic groups can be distinguished: (a) for Ln = La, Eu, Ce^{4+}, and Tm the signal is solely due to Cu^{2+} spins as the rare-earth spin vanishes in the ground state; (b) in the case of Ln = Gd the gadolinium spin dominates the absorption; (c) for Ln = Pr and Nd the Cu^{2+} signal dominates the spectrum, while the Ln signal is weak; (d) both ions yield sizable contributions to the absorption in $Er_{2/3}Cu_3Ti_4O_{12}$ and the remaining compounds.

To start with group (a) the spectra of $La_{2/3}Cu_3Ti_4O_{12}$ (with La^{3+} in a $4f^0$ electron configuration) consist of a symmetric resonance line in the paramagnetic regime, but reveal a clear asymmetry in the magnetically ordered phase. The signal is well described by two Lorentz curves of different linewidth but comparable intensity and approximately the same resonance field corresponding to a g value $g = h\nu/\mu_B H_{res} \approx 2.16$, typical for Cu^{2+} where the orbital momentum is nearly quenched by the ligand field [27]. The temperature dependence of the fit parameters – intensity, resonance field, and linewidth – is depicted on the left side of Fig. 8. In the paramagnetic regime the ESR intensities of both contributions follow very similar Curie-Weiss laws, which sum up to the static susceptibility probed by SQUID measurements. The antiferromagnetic transition at T_N appears as a sharp kink followed by a drop of the intensity to lower temperatures again in agreement with the static susceptibility. The resonance fields H_{res} remain approximately constant in the paramagnetic regime, but clearly shift to lower fields below T_N due to internal fields in the ordered phase. At high temperatures the linewidth ΔH attains values of about 250 Oe and 650 Oe for the narrow and the wide contribution, respec-

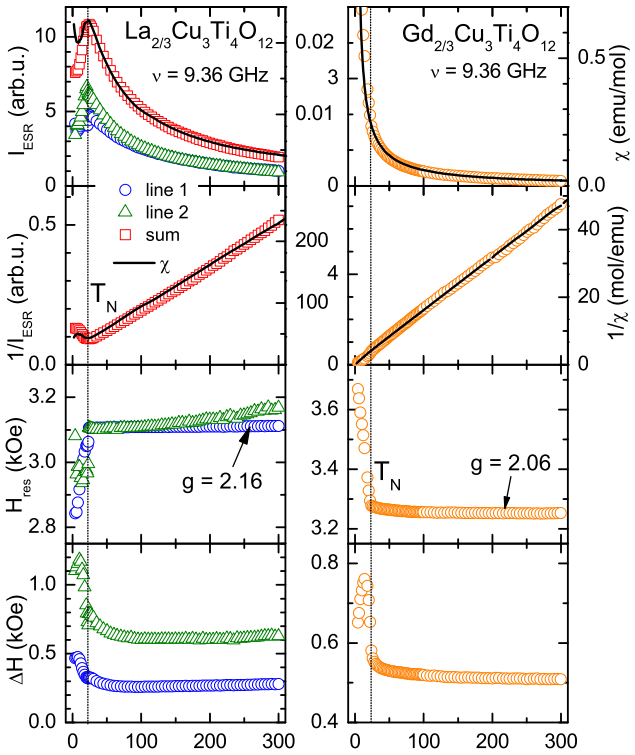

Fig. 8. (Color online) Temperature dependence of ESR intensity (symbols) compared to SQUID susceptibility (solid lines), inverse intensity and susceptibility, resonance field and linewidth in $La_{2/3}Cu_3Ti_4O_{12}$ (left frame) and $Gd_{2/3}Cu_3Ti_4O_{12}$ (right frame).

tively. On approaching magnetic ordering the linewidth increases only slightly driven by critical spin fluctuations but changes more pronounced having passed T_N into the ordered phase.

The linewidth behaves similar to that observed in $CaCu_3Ti_4O_{12}$, which was recently investigated in detail by Pires *et al.*, who performed systematic annealing experiments using O_2 or Ar atmosphere [28]. In that work it was found that the main source of line broadening stems from the dipolar interaction between neighboring Cu^{2+} spins as well as with some Ti^{3+} spins generated by oxygen vacancies, whereby the exchange interaction results in strong exchange narrowing of the signal. As grown or O_2 annealed $CaCu_3Ti_4O_{12}$ samples exhibit a linewidth of about 40 Oe, which results from Cu–Cu dipolar broadening, only, where practically no oxygen vacancies exist. But Ar annealing increases the linewidth by a factor of 5, because oxygen is extracted from the sample leaving paramagnetic Ti^{3+} instead of diamagnetic Ti^{4+} switching on the dipolar interaction between Cu^{2+} and Ti^{3+}, whereby the Cu–Ti distance is significantly smaller than the Cu–Cu distance. In $Ln_{2/3}Cu_3Ti_4O_{12}$ probably disorder plays an additional role for the line broadening, because only 2/3 of the lanthanide sites are randomly occupied leading to different local coordination of the Cu spins. This may be the main reason for the necessity to fit the ESR signal by the superposition of two Lorentz lines of comparable intensity but different linewidth, which approximately accounts for the spatial fluctuations of the local interactions due to disorder. Because of the all over cubic crystal symmetry and the dominant exchange coupling between Cu sites of different local anisotropy axis, the usual explanation for the existence of two signal components in the powder pattern at g values $g_{||}$ and $g_\perp$ for the magnetic field applied parallel and perpendicular to the local anisotropy axis can be ruled out.

A similar behavior like in the La compound is obtained for the Eu system, where the rare-earth spin is zero in the ground state due to Hund's rule. Again the spectra are best described by two lines with slightly lower g values 2.12 and 2.14 and comparable linewidths of 490 Oe and 260 Oe, respectively. In the Tm compound, which exhibits a zero-spin ground state at low temperatures due to the crystal-field splitting, even one Lorentz line nicely fits the ESR spectrum with $g \approx 2.1$ and $\Delta H \approx 750$ Oe in the paramagnetic regime. In $Ce_{1/2}Cu_3Ti_4O_{12}$ the signal is satisfactorily described by a broad single resonance line at $g \approx 2.24$, which increases in width from 2 kOe at room temperature to 3 kOe just above T_N. In the latter two compounds the signal is additionally broadened by the dipolar interaction with the Tm^{3+} spins of the excited states and with about 10% Ce^{3+} spins detected also by specific heat, respectively.

For $Gd_{2/3}Cu_3Ti_4O_{12}$ – case (b) – the ESR spectrum is well described by a single Lorentz curve in the whole temperature range. The resonance field at $g = 2.06$ and linewidth behave similar to $La_{2/3}Cu_3Ti_4O_{12}$, with a distinct kink at T_N, however the ESR intensity does not show any anomaly at T_N. This signal has to be attributed mainly to the Gd^{3+} spins $S = 7/2$, which stay paramagnetic even in the antiferromagnetically ordered regime and, hence, follow the Curie-Weiss law down to low temperature, while resonance field and linewidth are sensitive parameters to the magnetic ordering of the Cu system. The Cu signal cannot be separated from the Gd signal, because its g value nearly coincides with Gd and the linewidth is comparable, but its intensity is about a factor of 5 weaker than that of the Gd signal. Nevertheless, the g factor of 2.06 indicates the admixture of the copper signal, because in insulating matrix Gd^{3+} is expected to reveal a g factor 1.993 [27], whereas $g = 2.16$ is observed, if only Cu^{2+} contributed to the resonance line.

Focusing on group (c) represented by $Pr_{2/3}Cu_3Ti_4O_{12}$ in the left column of Fig. 9, the ESR spectra are satisfactorily described by a single Lorentz line at resonance fields corresponding to $g \approx 2.2$ with the linewidth increasing from about 2 kOe at room temperature up to 3 kOe and 4 kOe at T_N for $Pr_{2/3}Cu_3Ti_4O_{12}$ and $Nd_{2/3}Cu_3Ti_4O_{12}$, respectively, plus a weak signal at a resonance field of about 0.7 kOe. Regarding the g-value the strong line can be ascribed to Cu^{2+}. Moreover, its inverse intensity yields a Curie-Weiss temperature of about $\Theta_{ESR} \approx -40$ K, clearly below the SQUID value, which is influenced by the Curie contribution of the rare-earth spins. The intensity of the low-field line is by far too weak to account for the full rare-earth spin and is approximately independent on temper-

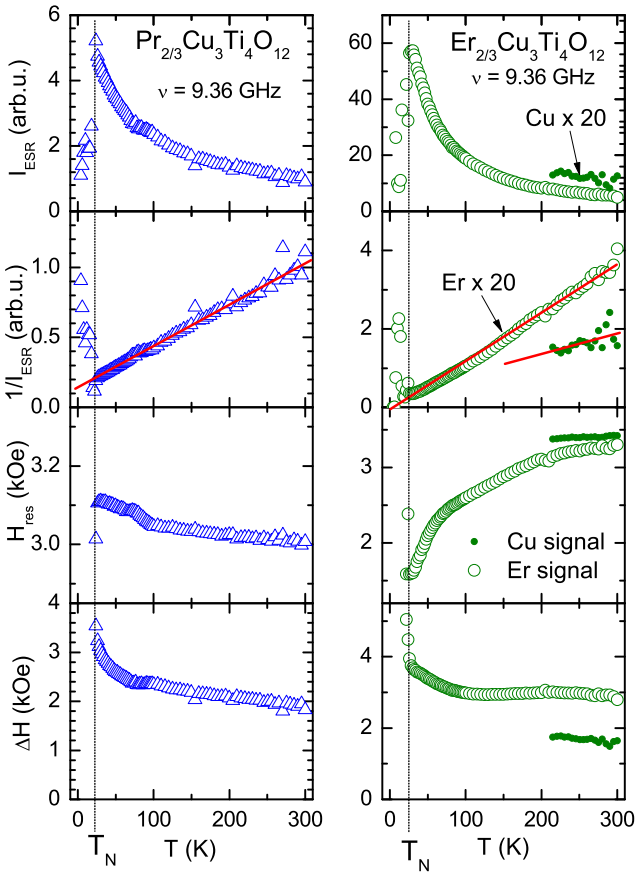

Fig. 9. (Color online) Temperature dependence of ESR intensity, inverse intensity, resonance field and linewidth in $Pr_{2/3}Cu_3Ti_4O_{12}$ (left frame) and $Er_{2/3}Cu_3Ti_4O_{12}$ (right frame). Solid lines in the inverse-intensity plots indicate the respective Curie-Weiss laws. For the Er compound the (inverse) intensity data of the (erbium) copper line have been magnified by a factor of 20.

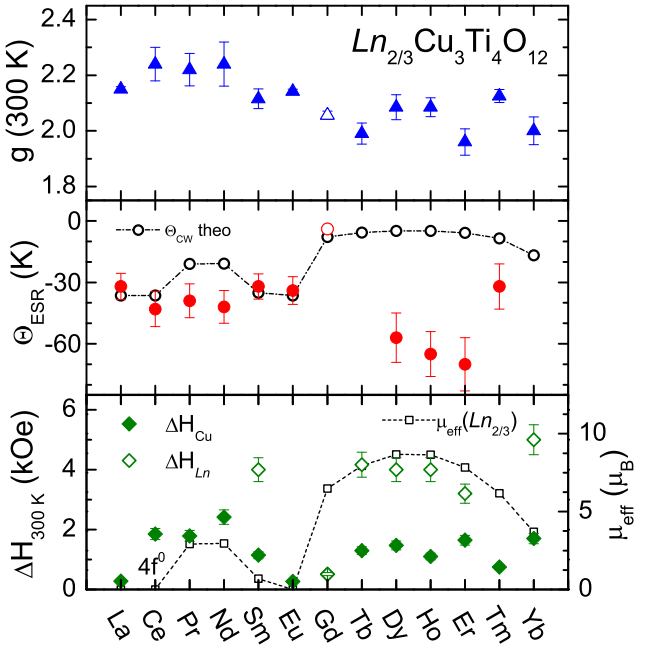

Fig. 10. (Color online) Evolution of g-value, Curie-Weiss temperature $\Theta_{\rm ESR}$, and room-temperature ESR linewidth $\Delta H_{300\rm K}$ determined from the copper signal (solid symbols) in $Ln_{2/3}Cu_3Ti_4O_{12}$ for different lanthanide ions. The open symbols indicate contributions of the rare-earth signal - for $Gd_{2/3}Cu_3Ti_4O_{12}$ the copper signal could not be distinguished from the Gd-signal.

ature. Probably this signal results from a small amount ($\ll 1\%$) of ferromagnetic impurities and, therefore, will not be further discussed. The rare-earth spin obviously does not give any measurable ESR signal. Likely due to spin-orbit coupling the relaxation of the rare-earth spin is so fast that the signal is too broad to be observable.

Concerning group (d) a reasonable separation of the different contributions to the ESR signal is possible in $Dy_{2/3}Cu_3Ti_4O_{12}$ and $Er_{2/3}Cu_3Ti_4O_{12}$, which is illustrated in the right column of Fig. 9. The copper signal is well resolved at $g \approx 2$ above 200 K. To lower temperatures the Er line dominates and itself exhibits a substructure due to the crystal-electric field which can be best fitted in terms of two Lorentzians, as visible in Fig. 7. But also a single Lorentz line yields a satisfactory description of the signal and was used for the present evaluation, because for a detailed investigation of the resonance field and substructure of the Er signal single crystals would be necessary. Here the most important information obtained is the signal intensity. At room temperature the copper intensity is one order of magnitude smaller than that of the erbium signal, as expected from ratio of the effective paramagnetic moments between Cu^{2+} and Er^{3+} (cf. Fig 5). Regarding the inverse intensities it is clearly visible that the copper signal follows a Curie-Weiss law with sizable negative Curie-Weiss temperature $\Theta_{\rm ESR} \approx -75$ K, while the erbium signal exhibits a pure Curie law. This again indicates that copper and rare-earth lattices can be independently treated. For the Ho and Sm compound the copper line can be extracted in a similar way to determine $\Theta_{\rm ESR}$, but the rare-earth contributions turn out to be more complicated probably due to the crystal-field splitting. Finally, for Tb and Yb one observes very broad spectra with a width ΔH of about 4 and 5 kOe, respectively, at resonance fields less than 2 kOe, which are superimposed by narrower lines of large amplitude at $g \approx 1.9$ due to small amounts of Ti^{3+} ions. The copper and rare-earth contributions can be identified at high temperatures, but a reliable termination of $\Theta_{\rm ESR}$ is not possible.

Figure 10 summarizes the relevant results of the ESR measurements in $Ln_{2/3}Cu_3Ti_4O_{12}$ dependent on the lanthanide ion. In all compounds with exception of $Gd_{2/3}Cu_3Ti_4O_{12}$ the copper signal could be identified to determine the g-value and Curie-Weiss temperature $\Theta_{\rm ESR}$ of the copper sublattice. The g-values vary around an average value $g_{\rm Cu} = 2.18$ in reasonable agreement with the susceptibility data, whereby it is slightly enhanced for the Ce, Pr, and Nd system but smaller for the heavy rare-earth compounds. The Curie-Weiss temperatures $\Theta_{\rm ESR}$ are in general lower than those determined from the SQUID mea-

surements, because they are not reduced by the Curie contribution of the rare-earth spins. Only for $Gd_{2/3}Cu_3Ti_4O_{12}$ the g-value and Curie-Weiss temperature is dominated by the gadolinium spins, because their g-value roughly coincides with the copper spins. Note that especially for the Eu compound we find the proper Curie-Weiss temperature $\Theta_{\mathrm{ESR}} = -34\,\mathrm{K}$ expected for the case of zero-spin Eu^{3+}, because the van-Vleck contributions of europium are not detected by ESR. Moreover, we observe larger absolute values of the Curie-Weiss temperature as compared to $La_{2/3}Cu_3Ti_4O_{12}$ in the heavy rare-earth compounds indicating some influence of the rare-earth ions on the exchange interaction in the copper system, although the ESR signal of the rare-earth spins can be identified independently, which proofs the general independence of the magnetic sublattices. Finally, the copper linewidth taken at room temperature shows a qualitative similarity with the effective paramagnetic moment, i.e. the local dipolar fields of the rare-earth spins enhance the spin-spin relaxation. For the heavy rare-earth compounds the enhancement seems to be smaller, probably due to the fact that the exchange-narrowing is larger than for the light rare-earth systems as anticipated from the larger absolute values of the Curie-Weiss temperature. The rare-earth signal can be mainly identified in the heavy rare-earth systems, but due to its huge linewidth of about 4 kOe and underlying crystal-field splittings for its deeper analysis high-field and -frequency ESR as well as single crystals would be necessary.

4 Conclusion

In this work we presented a detailed structural, magnetic, and thermodynamic characterization of $Ln_{2/3}Cu_3Ti_4O_{12}$ where Ln stands for the lanthanides including La, Ce, Pr, Nd, Sm, Eu, Gd, Tb, Dy, Ho, Er, Tm, and Yb. All polycrystalline samples crystallize in space group $Im\bar{3}$. Most of the compounds were x-ray single phase. Traces of impurity phases ($< 2\%$) were detected in the Gd, Er, and Tm compounds. Larger volume fractions of impurities ($\sim 5\%$) were identified for Ln = Ce and Yb. The lattice constants of the cubic cell nicely follow the lanthanide contraction, with the exception of $Ce_{1/2}Cu_3Ti_4O_{12}$. The significantly too small lattice constant indicates the presence of the smaller Ce^{4+} ion, resulting in a 50% occupation of the A site only, to achieve charge neutrality.

The magnetic susceptibilities can nicely be described with a two-sublattice model, with the copper spins $S = 1/2$ ordering at 25 K and the rare-earth moments remaining paramagnetic down to the lowest temperatures. The susceptibility of $Tm_{2/3}Cu_3Ti_4O_{12}$ saturates at low temperatures indicative for a non-magnetic ground state of the crystal-field split $4f$ manifold. In all systems the rare-earth ions are fully decoupled from each other. In the compounds with heavy rare-earth ions a small coupling seems to exist between the copper spins and the rare-earth ions. The copper ions are in a $3d^9$ configuration and their g value is about 10% enhanced with respect to the free electron value due to spin-orbit coupling.

Heat capacities between 2 K and 50 K were investigated for Ln = La, Ce, Pr, Eu, Ho, and Tm. All compounds reveal a clear anomaly close to 25 K indicative for antiferromagnetic ordering of the copper spins. The ordering temperatures of the heavy rare-earth compounds are slightly shifted towards higher temperatures ($\sim 2\,\mathrm{K}$). Crystal-electric field excitations have been detected for the Pr, Ho, and Tm compounds. The former two can be interpreted due to a low-lying triplet. $Tm_{2/3}Cu_3Ti_4O_{12}$ with singlet ground-state magnetism reveals a singlet-singlet transition close to 20 K. A small crystal-field contribution was also identified in $Ce_{1/2}Cu_3Ti_4O_{12}$. Whether this contribution is due to an impurity phase or Ce exist in both valences (Ce^{3+} and Ce^{4+}) is still unclear in this compound.

Electron spin resonance allowed to identify the copper signal in most of the $Ln_{2/3}Cu_3Ti_4O_{12}$ compounds and to extract the corresponding g-values and Curie-Weiss temperatures Θ_{ESR} of the copper sublattice complementary to the SQUID measurements. Moreover, the onset of magnetic order is clearly observed in the ESR parameters in agreement with the specific-heat experiments. The copper linewidth is strongly affected by disorder due to the incomplete occupation of the A place. Moreover, a qualitative relation with the effective rare-earth moment is observed, indicating the spin-spin relaxation channel between rare-earth spins and copper spins via the magnetic dipolar interaction.

We thank Dana Vieweg for the SQUID measurements. This work was supported by the Commission of the European Communities, STREP: NUOTO, NMP3-CT-2006-032644 and by the Deutsche Forschungsgemeinschaft (DFG) via the Transregional Collaborative Research Center TRR 80 (Augsburg / Munich) and the Research Unit FOR 960.

References

1. A. N. Vasil'ev, O. S. Volkova, Low Temp. Phys. **33**, (2007) 895.
2. C. C. Homes, T. Vogt, S. M. Shapiro, S. Wakimoto, A. P. Ramirez, Science **293**, (2001) 673.
3. M. A. Subramanian, D. Li, N. Duan, B. A. Reisner, A. W. Sleight, J. Solid State Chem. **151**, (2000) 323.
4. D. C. Sinclair, T. B. Adams, F. D. Morrison, A. R. West, Appl. Phys. Lett. **80**, (2002) 2153.
5. P. Lunkenheimer, R. Fichtl, S. G. Ebbinghaus, A. Loidl, Phys. Rev. B **70**, (2004) 172102.
6. P. Lunkenheimer, S. Krohns, S. Riegg, S. G. Ebbinghaus, A. Reller, A. Loidl, Eur. Phys. J. Spec. Top. **180**, (2010) 61.
7. Z. Zeng, M. Greenblatt, M. A. Subramanian, M. Croft, Phys. Rev. Lett. **82**, (1999) 3164.
8. R. Weht, W. E. Pickett, Phys. Rev. B **65**, (2002) 014415.
9. W. Kobayashi, I. Terasaki, J. Takeya, I. Tsukada, Y. Ando, J. Phys. Soc. Jpn **73**, (2004) 2373.
10. A. Krimmel, A. Guenther, W. Kraetschmer, H. Dekinger, N. Buettgen, A. Loidl, S. G. Ebbinghaus, E.-W. Scheidt, W. Scherer, Phys. Rev. B **78**, (2008) 165126.

11. A. Krimmel, A. Guenther, W. Kraetschmer, H. Dekinger, N. Buettgen, V. Eyert, A. Loidl, D. V. Sheptyakov, E.-W. Scheidt, W. Scherer, Phys Rev. B **80**, (2009) 121101(R).
12. N. Buettgen, H.-A. Krug von Nidda, W. Kraetschmer, A. Guenther, S. Widmann, S. Riegg, A. Krimmel, A. Loidl, J. Low Temp. Phys. **161**, (2010) 148.
13. Y. W. Long, N. Hayashi, T. Saito, M. Azuma, S. Muranaka, Y. Shimakawa, Nature **458**, (2009) 60.
14. A. Deschanvres, B. Raveau, F. Tollemer, Bull. Soc. Chim. Fr. **11**, (1967) 4077.
15. B. Bochu, M. N. Deschizeaux, J. C. Joubert, A. Collomb, J. Chenavas, M. Marezio, J. Solid State Chem. **29**, (1979) 291.
16. M. A. Subramanian, A. W. Sleight, Solid State Sci. **4**, (2002) 347.
17. J. J. Liu, C. G. Duan, W. N. Mei, R. W. Smith, J. R. Hardy, J. Appl. Phys. **98**, (2005) 093703.
18. J. Sebald, S. Krohns, P. Lunkenheimer, S. G. Ebbinghaus, S. Riegg, A. Reller, A. Loidl, Solid State Commun. **150**, (2010) 857.
19. S. Krohns, J. Lu, P. Lunkenheimer, V. Brize, C. Autret-Lambert, M. Gervais, F. Gervais, F. Bouree, F. Porcher, A. Loidl, Eur. Phys. J. B **72**, (2009) 173.
20. V. Brize, C. Autret-Lambert, J. Wolfman, M. Gervais, P. Simon, F. Gervais, Solid State Science **11**, (2009) 875.
21. Y. J. Kim, S. Wakimoto, S. M. Shapiro, P. M. Gehring, A. P. Ramirez, Solid State Commun. **121**, (2002) 625.
22. A. Koitzsch, G. Blumberg, A. Gozar, B. Dennis, A. P. Ramirez, S. Trebst, S. A. Wakimoto, Phys. Rev. B **65**, (2002) 052406.
23. A. P. Ramirez, G. Lawes, D. Li, M. A. Subramanian, Solid State Commun. **131**, (2004) 251.
24. I. Terasaki, M. Iwakawa, T. Nakano, A. Tsukuda, W. Kobayashi, Dalton Transactions **39**, (2010) 1005.
25. B. R. Cooper, Phys. Rev. **163**, (1967) 444.
26. J. Hemberger, F. Schrettle, A. Pimenov, P. Lunkenheimer, V. Yu. Ivanov, A. A. Mukhin, A. M. Balbashov, A. Loidl, Phys. Rev. B **75**, (2007) 035118.
27. A. Abragam, B. Bleaney, *Electron Paramagnetic Resonance of Transition Ions*, (Clarendon Press, Oxford, 1970).
28. M. A. Pires, C. Israel, W. Iwamoto, R. R. Urbano, O. Agüero, I. Torriani, C. Rettori, P. G. Pagliuso, Z. Le, J. L. Cohn, S. B. Oseroff, Phys. Rev. B **73**, (2006) 224404.